Equatorial Ionosphere Characterization for Sub-Saharan Africa SBAS

Etienne Foucault, Pierre-Louis Blelly, Aurélie Marchaudon, Institute of Research in Astrophysics and Planetology, *Toulouse, France*

Damien Serant, Sébastien Trilles, *THALES ALENIA SPACE, Toulouse, France*

BIOGRAPHY (IES)

Etienne Foucault is a Ph. D. student in Astrophysicis working at IRAP (Institut de Recherche en Astrophysique et Planétologie), Toulouse, France, currently working on High frequency radio wave propagation in the mid latitude Earth's ionosphere.

Dr. Damien Serant is a research and development system engineer in Thales Alenia Space France since 2011, where he is involved in GNSS signal processing, INS hybridization, ionosphere studies on GNSS and full software GNSS receiver. He has graduated in 2008 as an electronics engineer from the ENAC (Ecole Nationale de l'Aviation Civile), Toulouse, France. He received his Ph.D in signal processing, in 2012 from the INPT, University of Toulouse, France.

Dr. Sébastien Trilles is a Navigation Expert with Thales Alenia Space. He received his Ph.D. degree in Pure Mathematics from the Paul Sabatier University, Toulouse (France) in 2000 and an Advanced M.S. in Space Technology from the ISAE, Toulouse, France in 2003. He is a specialist in navigation algorithms concept and design.

Dr. Pierre-Louis Blelly is a permanent CNRS researcher at IRAP (Toulouse, France). He is graduated from Ecole Polytechnique and Ecole Nationale Supérieure de l'Aéronautique et de l'Espace. He is a specialist in numerical modelling of terrestrial ionosphere and developed numerous models, the TRANSCAR/IPIM family models, which are now acknowledged as reference models for the study of the high latitude ionosphere.

Dr. Aurélie Marchaudon is a permanent CNRS researcher at IRAP (Toulouse, France). Her work has been dedicated to a better understanding of the magnetosphere-ionosphere coupling by combining ground-based instrumentation like SuperDARN radars and space-borne instruments and simulation from ionosphere models (TRANSCAR, IPIM). Since 2008, she is the SuperDARN PI of the French Kerguelen radar.

ABSTRACT

Performance Based Navigation (PBN) is a concept developed by ICAO (International Civil Aviation Organization) that specifies the operational performance required in an airspace, route or approach procedure. A Satellite Based Augmentation System (SBAS) enhances the performances of the existing satellite navigation system. It is used to deploy Global Navigation Satellite System (GNSS) approach for PBN procedures. The required performance level for vertical guidance is directly linked to approach category criteria. The real performance provided by an SBAS for a single-frequency user depends on the physical characteristics of the ionospheric layer. As Sub-Saharan Africa corresponds to geomagnetic equator region, the question of ionosphere dynamics characterization in equatorial zone is central to gauge what SBAS performance level can be achievable.

In the equatorial zone the dynamics of the ionosphere is subject to complex physical phenomena, involving rapid recombination of ion-electron pairs. Moreover these phenomena are transient with high local spatial and temporal gradients. These zones promote the occurrence of scintillation phenomena, bubbles (strong local fall of TEC (Total Electron Content)), and small scale gradients, which must be evaluated for the ionosphere modeling and integrity data generation.

Based on a large volume of GNSS measurements covering more than four years of data collected, Thales Alenia Space associated with IRAP (Astrophysics and Planetology Research Institute, Toulouse, France), present a panorama of observed physical events through the ionosphere in Sub-Saharan Africa zone. The main purpose of this study is to establish a clear view on the physical mechanisms that drive the equatorial ionosphere dynamics and the effects on GNSS measurements. This study

is supported by information coming from TEC values, TEC gradients amplitudes, and the nature of scintillation events as intensity, impact area and occurrence in time.

Conclusion of these activities is to highlight that ionosphere conditions above sub-Saharan area are consistent with the performances level of SBAS approach with vertical guidance. Indeed scientific analyses show that a precise service level is possible on this zone with a very good level of availability above the main airports.

INTRODUCTION

With the development of long range communication and Global Positioning System (GPS), a worldwide coverage becomes available. Industrial use of GPS positioning such as precise point positioning has also profited from this development. Safety of life algorithm was already in use for North American Flight Aviation (WAAS) or in Europe with EGNOS (European Geostationary Navigation Overlay System). Currently, the main source of single frequency GPS measurements error is the ionosphere, because of its effects on the propagation of radio wave signals. Position accuracy of users with single-frequency signal is directly affected by these errors. Mid-latitude ionosphere shows sufficiently low and slow variation of ionospheric quantities to allow the use of such a GPS regional augmentation system. Interrogations are raised regarding the development of such system in the region of the geomagnetic equator, which is known to host more perturbative processes.

In this paper, we present a study of the equatorial ionosphere based on the data monitored by the SAGAIE network of stations from 2014 to 2017. SAGAIE is a project funded by the Centre National d'Etude Spatiale (CNES - French Space Agency) in cooperation with ASECNA. The objective of SAGAIE was to assess the feasibility of an SBAS in sub-Saharan equatorial region by a better characterization of the ionosphere activity in the zone (scintillation, high electron density gradient, bubbles…). To probe the ionosphere layer over the area of interest, SAGAIE has deployed from mid-2013 and maintain a network of GNSS stations to collect raw GNSS measurements. The SAGAIE network is composed of 5 stations and has been complemented in mid-2015 by 4 stations in the frame of the MONITOR project (ESA – European Space Agency). The stations are operated by ASECNA. A description of the network can be found in [1].

To begin with, a short reminder of the ionosphere formation and structure is presented. Then in the second section, the equatorial ionosphere properties are described. In the third section, study results are analyzed and then discussed. Finally a conclusion of the equatorial ionosphere study is proposed.

IONOSPHERE

The Earth's ionosphere is a part of the atmosphere, ranging typically from 60 km to 3000 km altitude. It is composed of ions and electrons, resulting from the ionization of atmosphere's neutrals by solar radiation. Historically, the ionosphere has been discovered because of its perturbative effect on radio wave propagation. Dense ionosphere regions lay between 100 and 500 km altitude.

The ionosphere is dependent from the Earth-Sun configuration and its properties evolve with respect to them. A strong link between ionization levels and solar cycle (i.e. solar irradiation) is observed. Also the ionosphere relates to the Earth's atmosphere, as it brings the needed particles to be ionized by solar irradiance.

In this section, we will briefly introduce the solar activity, then discuss the ionosphere formation and finally, describe the main regions of interest in the ionosphere. Presentation is based on [2].

Solar activity

The solar cycle activity follows an 11-year cycle. Last solar activity maximum was registered in 2014 and the next one is awaited for 2025. We are now at the end of solar cycle 24. A proxy of solar activity is F10.7 index which evolution for solar cycle 23 and 24 is shown on **Figure *1***. Solar activity is characterized by the variability of the solar flux, especially in the EUV/XUV range (0.1-100 nm). This part of the solar spectrum is responsible for the ionization of the neutral species in the upper atmosphere and thus is a critical parameter for the ionosphere. Some proxies have been developed for measuring this activity and all have the same behavior with an eleven year periodicity. With this respect we have plotted on **Figure *1*** F10.7, MgII index and Sunspot number for the solar cycles 23 and 24. There is a strong correlation between them, F10.7 is one historical index chosen to characterize this activity and is used to parameterize the solar flux in the EUV/XUV range. Bottom panel of **Figure *1*** presents the evolution of the solar flux irradiance in the range (0.1-100 nm) derived from FISM (Fare Irradiance Spectral Model) [3], during the two cycles. There is a clear correlation with solar indices.

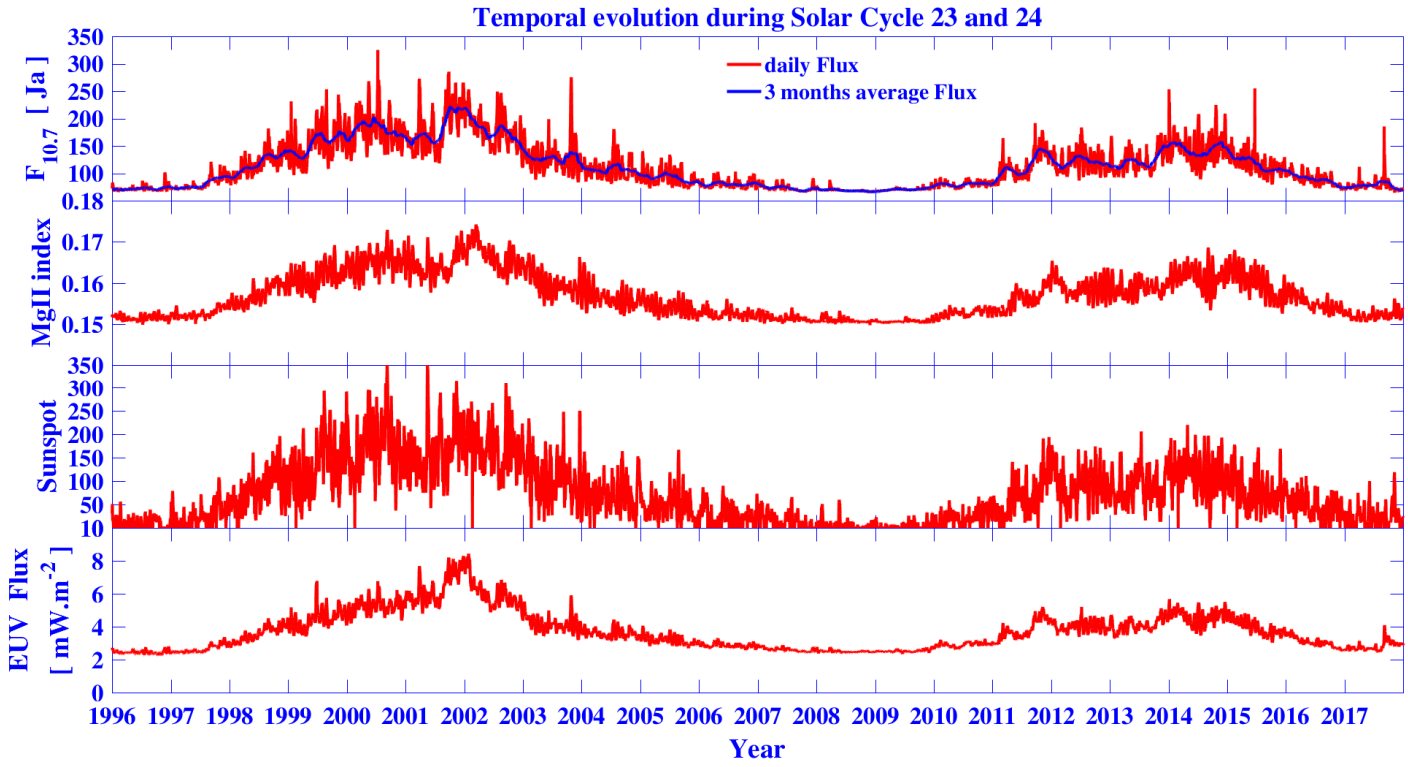

Figure 1: Temporal evolution of different solar activity proxy during solar cycles 23 and 24. From up to bottom is presented the solar flux F10.7 daily variation (in red) and the 3-month averaged variation (in blue), the MgII ray index, the sunspot number and the EUV solar irradiance (0.1-100 nm).

Ionosphere formation

The ionosphere is the product of the interaction between solar radiation and Earth's atmosphere. The upper part of the atmosphere acts as a shield, absorbing most of the radiation and incident particles. Absorption leads to excitation of the neutral component as some energy is lost by the incident radiation. If the energy received by the neutral is sufficient, an electron will be stripped from it, creating an ion-electron pair. When the radiation flux are high enough (i.e. during the day) a large number of ion-electrons pairs are created, forming a plasma, with a maximum density around approximately 250km. This is the so-called ionosphere.

As the neutral components change with respect to the altitude and as the absorption rates also vary with altitude, the ionosphere is structured in different layers. In this study, the assumption of gravitational balance is taken. We suppose each atmospheric component in hydrostatic equilibrium. Therefore, if we also suppose the gravity field g uniform along the altitude and an isotherm atmosphere, we can write the concentration profile over altitude z of a specie n as:

$$n_n(z) = n_n^0 e^{\left\{-\frac{m_0 g}{k_b T_n}(z-z_0)\right\}} = n_n^0 e^{\left\{-\frac{z-z_0}{H_n}\right\}}$$

Where n_n^0 is the concentration level of the specie n at the reference altitude z_0, k_b is the Boltzmann constant and $H_n = \frac{k_b T_n}{m_0 g}$ is the scale height of the species n. Atmospheric profiles are displayed in **Figure *2***. It shows the dominant molecular species at lower altitude and atomic species at high altitude because of the gravitational filtering. The major ionization source is the solar irradiance (UV light).

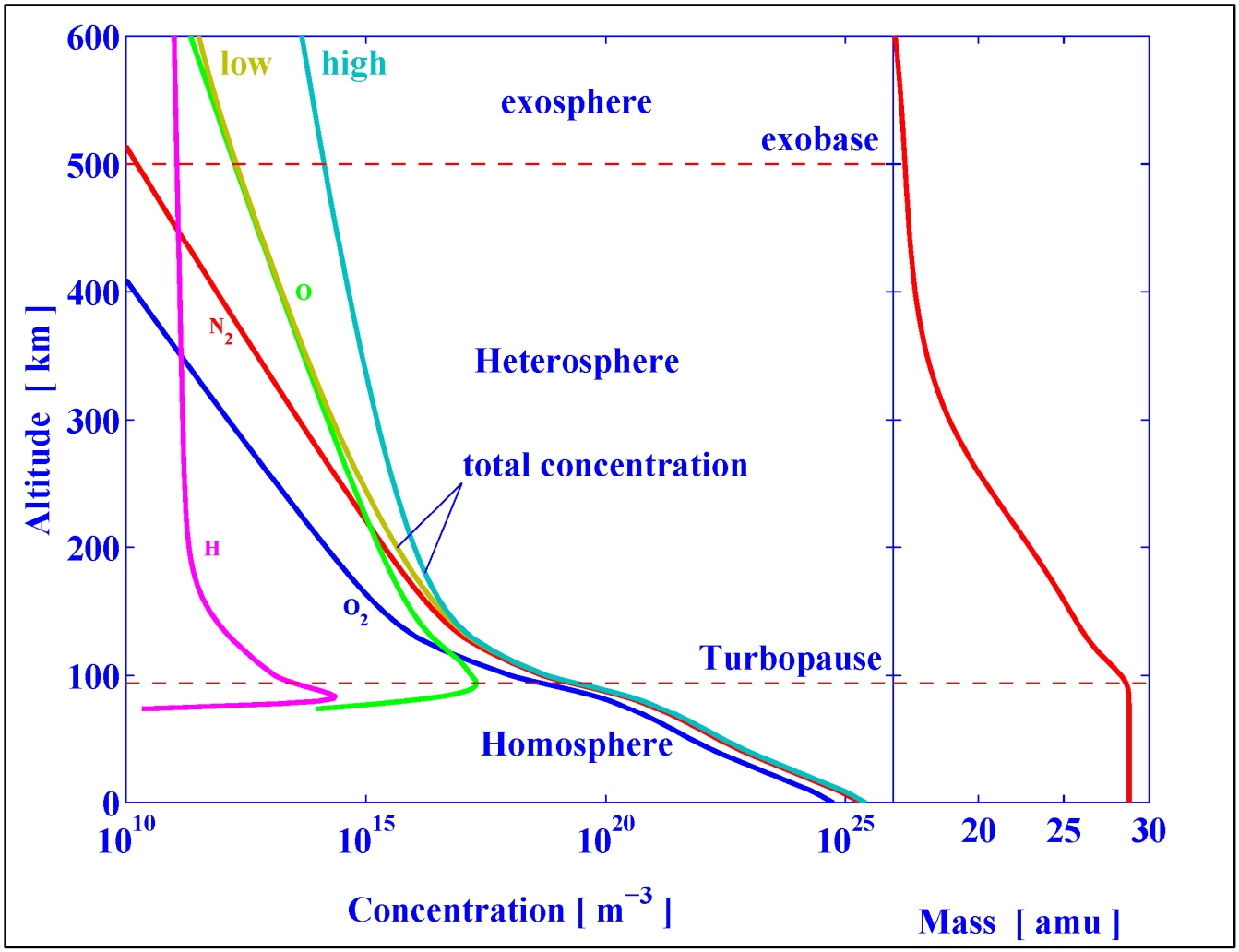

Figure 2: Atmosphere Vertical Profile

Ionosphere structure

The ionosphere is divided in different layers, depending on the altitude. Main ionosphere “regions” or “layers” are the D region (60 to 90 km altitude), E region (90 to 150 km) and the F region (150 to 500 km). Those regions are defined with respect to the main processes and mechanisms governing them, and also because of their chemistry composition. Electron density profile with respect to altitude is displayed in **Figure *3***.

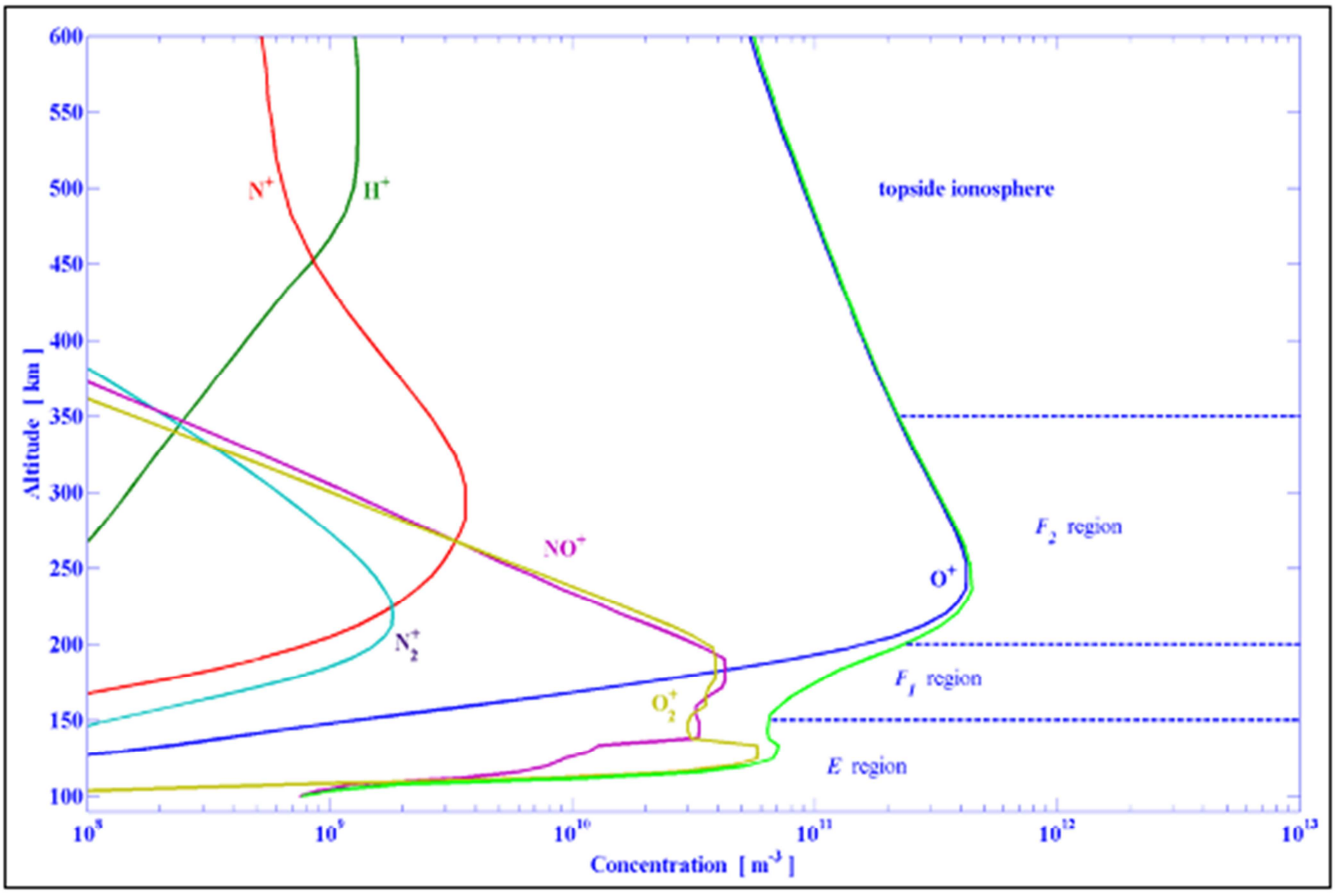

Figure 3: Density profile of ionospheric species, depending on altitude

EQUATORIAL IONOSPHERE PROPERTIES

At the equator, local physical processes develop in the ionosphere, mainly caused by the magnetic field line geometry. In order to understand the profile monitored by the GPS navigation data, it is important to review these ionospheric properties. First we describe the equatorial electrojet, which is an electrical current parallel to the magnetic equator. Then we present the equatorial fountain, a wide convective movement. Finally, we present the equatorial plasma bubbles, an evening feature of the equatorial ionosphere, which cause rapid TEC variations.

Equatorial Electrojet

The main property of the equatorial ionosphere is an electrical current flowing parallel to the magnetic equator. It is flowing eastward on the day side, and westward on the night side and is driven by neutral wind. Solar illumination heats the equatorial upper atmosphere. The temperature gradient between the dawn and evening side generates a strong eastward wind. In the lower part of the ionosphere, the movement of the ions is driven by the collisions with the neutrals while the electrons are trapped around magnetic field lines. Therefore, ions also move eastward, driven by the eastward neutral wind. This difference of behavior between ions and electrons implies a drift velocity $\vec{V_i} - \vec{V_e}$ between species which creates an electrical current:

$$\vec{j} = N_e e\left(\vec{V_i} - \vec{V_e}\right)$$

named the Equatorial Electrojet (EEJ). A worldwide estimation of its location is shown in **Figure *4***. We clearly see the electrojet is located in a narrow region collocated with magnetic equator. A more detailed study of the equatorial electrojet can be found in [4].

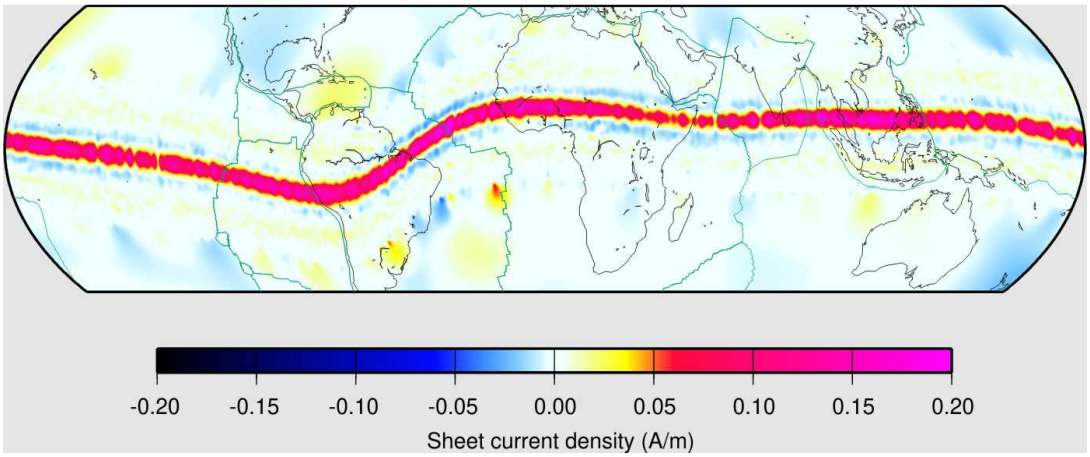

Figure 4: Worldwide electrojet monitoring *[4]*.

Equatorial Fountain

The magnetic field lines at the equator are almost horizontal and northward. The presence of the Equatorial Electrojet, and the Earth magnetic field $\vec{B}$ induce in the upper part of the ionosphere a vertical movement, which is the same for all charged species:

$$\vec{V} = \frac{\vec{E} \times \vec{B}}{B^2}$$

Plasma is transported upward, uplifting lower regions of the ionosphere at higher altitudes. This motion is perpendicular to $\vec{B}$, but the movement of the particles follows the magnetic field lines and eventually, gravity acceleration will catch up the effect and bring down the particles still following magnetic field lines. Hence creating an accumulation of the electron density on latitude ±15° and a depletion at the equator. This phenomena is called Appleton Anomaly or also equatorial fountain due to its shower-like movement. This process is illustrated in **Figure *5***. Further development and precision of the Equatorial Fountain mechanism can be found in [5].

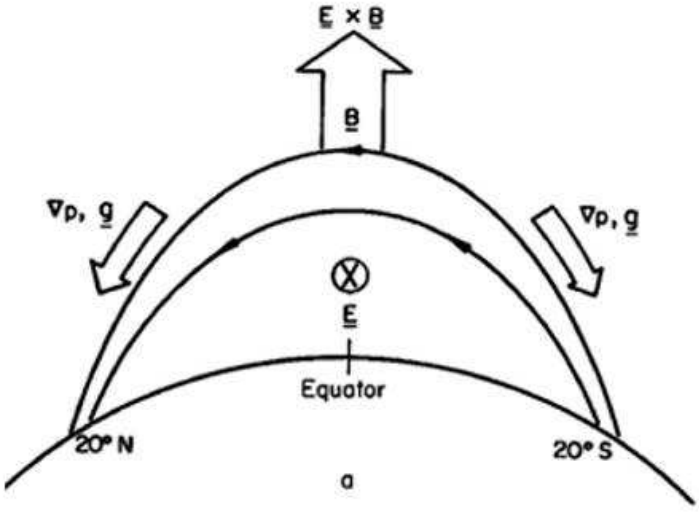

Figure 5 : Equatorial fountain process scheme *[6]*

Equatorial Plasma Bubbles

As we have defined the equatorial fountain we can now introduce the main source of perturbation for radio signal propagation in the equatorial region: the Equatorial Plasma Bubbles (EPB). They are created when a large amount of electrons is uplifted by the fountain effect, which occurs preferably in the evening, before the EEJ inversion. As the EEJ is about to reverse a sudden and short increase of the electrical current amplitude is observed, accelerating the fountain effect. As the Sun goes

down, recombination process starts at lower altitude, where the collision rate is important, while the uplifted particles will stay ionized longer due to a lower collision rate. Ionosphere is then separated into two different regions: one at lower altitude with lower electron density due to the recombination enhancement, and a second at upper altitude where recombination is delayed due to the amount of plasma transported by the fountain effect. This density gradient may create a Rayleigh-Taylor instability, driving the generation of plasma bubbles, which are bubbles of tenuous electron density moving upward, or, bubbles of dense electron density moving downward. Those bubbles create strong TEC gradients along the GNSS satellite line-of-sight and produce high scintillation, impacting the propagation of radio wave signals at sunset. Equatorial plasma bubbles have been simulated by [7], a result is shown in **Figure *6***.

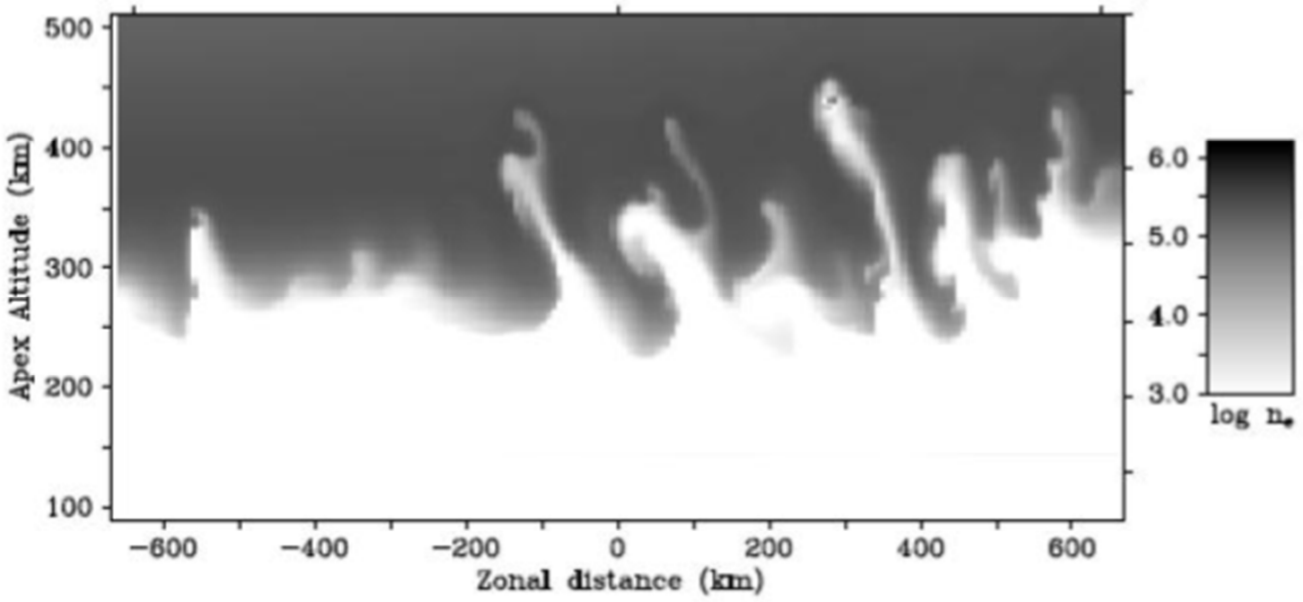

Figure 6: Plasma bubbles simulation *[7]*

METHOD

In this section, we introduce the ionospheric quantities we have been looking to for this study. First of all, we introduce the Total Electron Content (TEC), the Along Arc TEC Rate (AATR) and finally the scintillation index S4.

Total Electron Content

One of the quantity we would like to follow is the variation of the electron density N_e. We define the Total Electron Content as the quantity of electron along the Line-of-Sight (LoS):

$$TEC = \int_L N_e dl$$

Where L is the optical length, N_e the electron density,dl a finite element of LoS. TEC is proportional to the ionization of the ionosphere, but it does not represent the variation in altitude.

Along Arc TEC Rate

For a later purpose of this study, we have to define the Along Arc TEC Rate (AATR), which is calculated as:

$$AATR = \frac{1}{M^2(E_l)} \frac{\mathrm{d}STEC}{dt}$$

Where $\frac{dSTEC}{dt}$ is the TEC temporal gradient, $M(E_l)$ is a weighted function proportional to the solar zenith angle.

Data

For this paper, we look at four years of data from the SAGAIE network deployed in the West Africa area. This network is collecting receiver raw measurements (in the form of Rinex (Receiver Independent Exchange Format) observation) since mid-2013. Every visible GNSS satellite observed during this time period has been sampled at 1 Hz sampling rate. List of the used stations is displayed below.

Station	**Antenna**	**Latitude (°)**	**Longitude (°)**	**Altitude (m)**
Dakar	Novatel	14.749	-17.492	67.202
Dakar	Septentrio	14.749	-17.492	67.202
Douala	Novatel	4.013	9.715	62.835
Lome	Novatel	6.168	1.252	69.638
Lome	Septentrio	6.168	1.252	69.638
Ndjamena	Novatel	12.128	15.033	316.765
Ouagadougou	Novatel	12.356	-1.513	377.48

Each station has monitored every navigation satellites from the following constellation:

- GALILEO: E1, E2, E5
- GPS: L1, L2, L5
- GLONASS: G1, G2
- BEIDOU: B1, B2

Using this database, Thales Alenia Space has selected data from the GPS constellation to compute the ionospheric properties. Pseudo range code and phase have been combined to estimate the TEC along each LoS. Considering a station *i* and a satellite *j*, we can define for every f_1 frequency measurement:

$$P1_j^i = D + \left(h1_j - h1^i\right) + e_j^i + T + \epsilon_1$$

And for frequency f_2 measurement:

$$P2_j^i = D + \left(h2_j - h2^i\right) + \gamma e_j^i + T + \epsilon_2$$

Where D is the geometric distance between the station *i* and the satellite *j*, *h1* and *h2* are the clock estimation error for f_1 and f_2 frequency respectively (pure clock offset plus hardware bias), *e* the ionospheric delay related to f_1 frequency, *T* the troposphere delay, ϵ is the residual error estimation containing multipath effects, and $\gamma = \frac{f_1^2}{f_2^2}$. The equation can be rewritten as:

$$P2_j^i = D + \left(h1_j - h1^i\right) + IFB_j - IFB^i + \gamma e_j^i + T + \epsilon_2$$

Where $IFB = h2 - h1$ and stands for Inter Frequency Bias. Knowing the *IFB*, let us compute the ionosphere delay *e* as:

$$e = \frac{P2_j^i - P1_j^i - IFB_j + IFB^i}{\gamma - 1}$$

For this study, Thales Alenia Space has been able to get the *IFB* estimation for the GPS constellation only. In the following, only the measurements made using this constellation are presented. To improve and compare the results obtained with this method, an estimation of the ionosphere properties using code and phase measurements would be necessary. From the ionosphere delay *e*, the TEC measurement has been derived:

$$TEC = e\ \frac{m_e \epsilon_0 f^2}{e_c^2}$$

Where e_c is the electron electric charge, m_e the electron mass and ϵ_O the permeability of free space. Finally to smooth the data obtained by this method, a mean computation over 60 seconds has been performed, using a Kalman filter. Final set of data is available at a time step of 1 minute.

Scintillation index S4

The scintillation index S4 measures the temporal variation of a signal intensity. The S4 index is defined as:

$$S_4 = \sqrt{\frac{< I^2 > - < I >^2}{< I >^2}}$$

Where <> represents the temporal mean over 60s, I is the intensity of a radio wave signal. During quiet time, the ionosphere profile has low variations, leading to very small changes in the received intensity. The S4 index is close to 0 as the absorption remains constant and low. However, during severe ionospheric events, ionospheric profile shows a rapid variation, leading to an increase of the S_4 index as the absorption increases. The signal absorption can be sufficient to prevent a user to receive the signal. Indeed below some intensity threshold, some receivers cannot proceed the information contained in the navigation signal, meaning inability for users to accurately be positioned. In this paper, we will consider that a scintillation index $S_4 \leq 0.3$ does not affect the reception of a signal, and a scintillation index $S_4 > 0.9$ will result in a fully absorbed signal.

LOW FREQUENCY VARIATIONS

Ionospheric ionization rates have temporal variations, mostly related to the solar illumination. The first step of this study is to investigate the different temporal variation rate, which play a role in the equatorial ionosphere formation. To do so, we present here the results for different time scale, going from hourly to annually.

Solar cycle

Annual variations are controlled by solar cycle. As the period chosen spans from early 2014 (solar maximum; F10.7≈140) to end of 2017 (solar minimum; F10.7≈70), the variations are representative of a declining phase of solar cycle (see **Figure *1***). Here we focus on TEC measurements average on a yearly basis. For all available stations considered and low elevations mask applied (elevation > 5°), we compute the mean values which are presented in **Figure *7***. TEC is plotted in TECU ($1\ TECU = 10^{18} e^-/m^3$) as a function of year. TEC standard deviation σ is also plotted. There is a clear correlation between TEC, σ and solar activity, decreasing from a maximum value reached at solar maximum to a minimum reached at solar minimum. This has already been evidenced by [8] who showed a strong correlation between maxima TEC values and solar activity. We can defined two state modes for the ionosphere, one which is quiet during the solar minimum and another one, “severe”, during solar maximum, where the ionosphere is expected to be more developed. During the rest of this study, we will try to find more evidence of this behavior in order to validate, or not, this hypothesis.

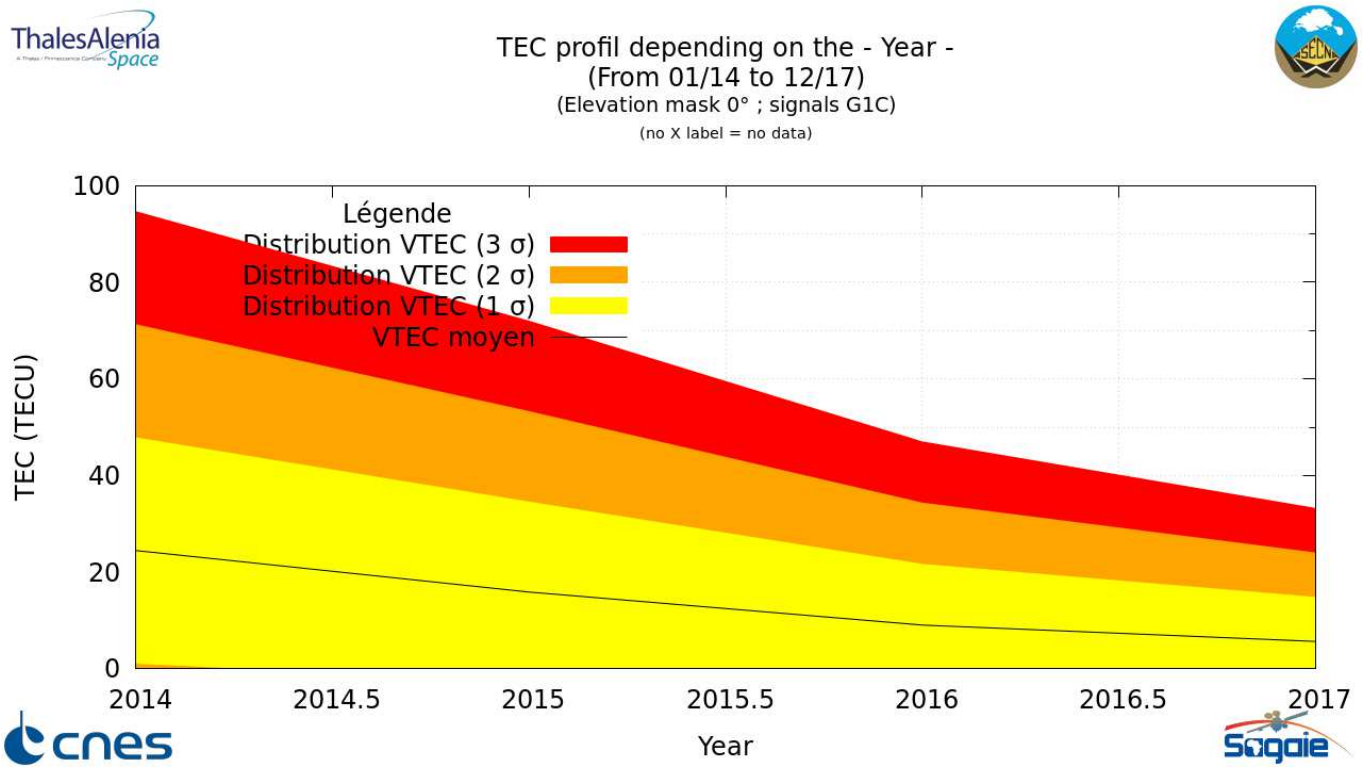

Figure 7: Annual mean TEC value from 2014 to 2017. Black line is $\|\boldsymbol{TEC}\|$, yellow bands are $\|\boldsymbol{TEC}\| +/ -\boldsymbol{\sigma}$, orange band is $\|\boldsymbol{TEC}\| + 2\boldsymbol{\sigma}$ and red band is $\|\boldsymbol{TEC}\| + 3\boldsymbol{\sigma}$.

Seasonal

The seasonal variation is related to Earth's orbit and the variation of declination angle δ, the angle between the geographic equator and the ecliptic. This declination controls the amplitude variation of solar zenith angle (SZA) χ which is the angle of the Sun direction with respect to the local vertical axis:

$$\cos(\chi) = \sin\delta \sin\lambda + \cos\delta \cos\lambda \cos h$$

Where λ is the geographic latitude and h is the hour angle:

$$h = TU + \frac{\phi}{15}$$

Where ϕ is the longitude.

Figure 8 shows the variation of the minimum solar zenith angle throughout the year for different latitudes. χ is an important parameter as it controls the absorption factor of solar radiation for a given location by means of the column density of neutral atmosphere passed through by the radiations. Low solar zenith angle means a high production rate and a low altitude for the maximum of production, while a high solar zenith angle means a low production rate and a high altitude for the maximum of production.

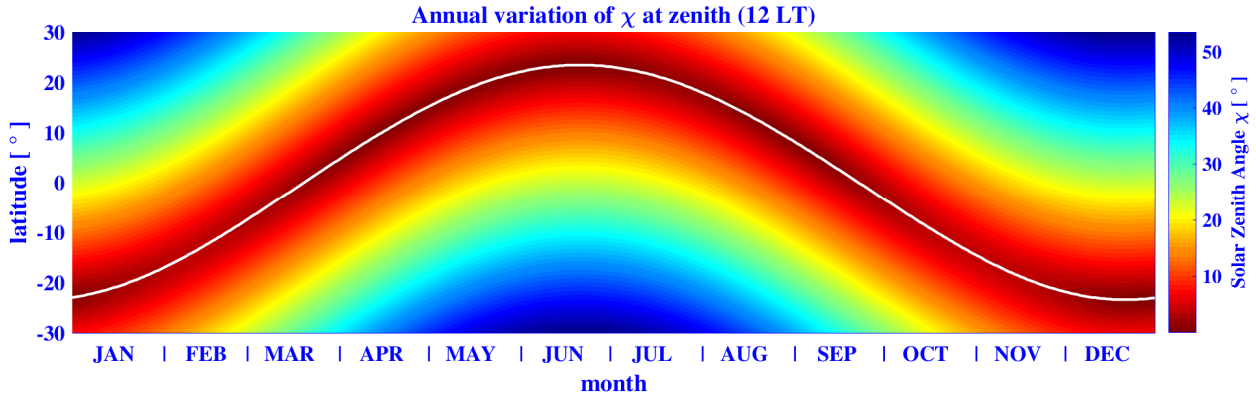

Figure 8: Annual Solar Zenith Angle Variation at different latitude. Solar zenith angle evolution is plotted in color, white line is the solar zenith angle being equal to 0°.

Figure *9* presents monthly TEC mean. There are two clear maxima around equinoxes and two minima close to solstices. As we are at equator, from **Figure *8*** we see that equinoxes correspond to the lowest χ value (≈0°) and solstices to the highest (≈27°) and thus production rate is higher at equinoxes than at solstices. Thus monthly TEC mean brings out this relationship between season and production. The variability is amplified by the seasonal evolution of neutral atmosphere. **Figure *10*** presents the annual evolution of the neutral concentration at 150 km for the two solar cycles, derived from the MSIS neutral atmosphere empirical model [9]. The concentration reaches a maximum at autumnal equinox and a minimum at summer solstice. Similar results have been found in previous study ([10], [11]).

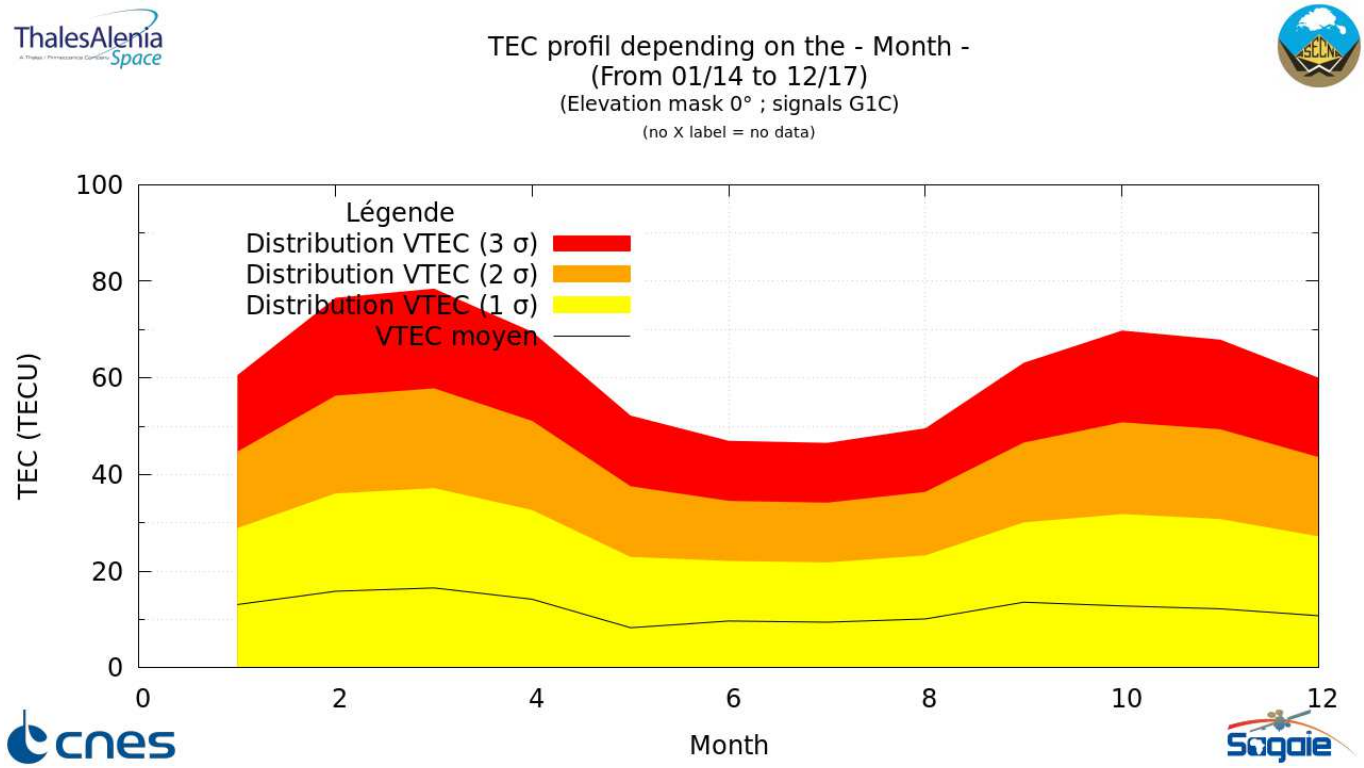

Figure 9: Monthly mean TEC value from 2014 to 2017. Black line is $\|TEC\|$, yellowbands are $\|TEC\| +/- \sigma$, orange band is $\|TEC\| + 2\sigma$ and red band is $\|TEC\| + 3\sigma$.

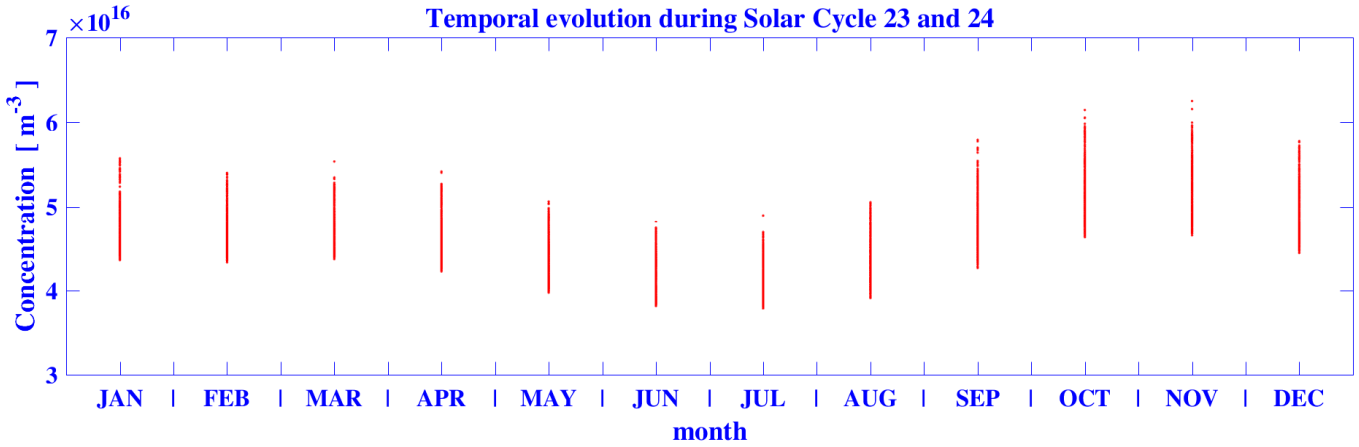

Figure 10: Monthly variation of the neutral concentration. Concentrations are calculated for the solar cycle 23 and 24, figure derived from *[9]*.

Daily

Finally, we have study the diurnal TEC variations. To do so, the data from each station were hourly averaged and a simple 24h mean for the 2014-2017 time interval was obtained. As the ionization process is controlled by solar radiation, ionosphere is supposed to be created from sunrise till sunset. Depending on the ionization rate at a specific day, ionosphere is expected to reduce during the night. Hourly average TEC is represented in **Figure *11*** as a function of local time, showing low value at the beginning of the day (from 00h to 6h), then a constant increase until 15h where it takes its maximum value, then a decrease. As expected, low TEC values are observed during night hours (from 23h to 05h), TEC increases during the day (from 06h to 15h) and then decays during the evening and night (from 15h to 05h). Previous study [8] suggested that the diurnal TEC variation is related to the small numbers of magnetic field tubes at low latitudes. As the total magnetic field tubes is small near the equator, the electron contents trap along them decay rapidly after sunset in response to the low temperature in the upper atmosphere during nighttime. When the sun rises, the magnetic field tubes are filled up quickly because of their low volumes resulting into a sharp increase in ionization.

However [12] suggested that the diurnal TEC variation may simply be caused by changes in the rates of electron production and loss in the ionosphere. At dawn, when the Sun rises, the ionization increases as the SZA decreases which leads to an increase of the electron concentration, with a maximum around local noon. During nighttime, since the primary source of ionization is no longer present, TEC values remain low.

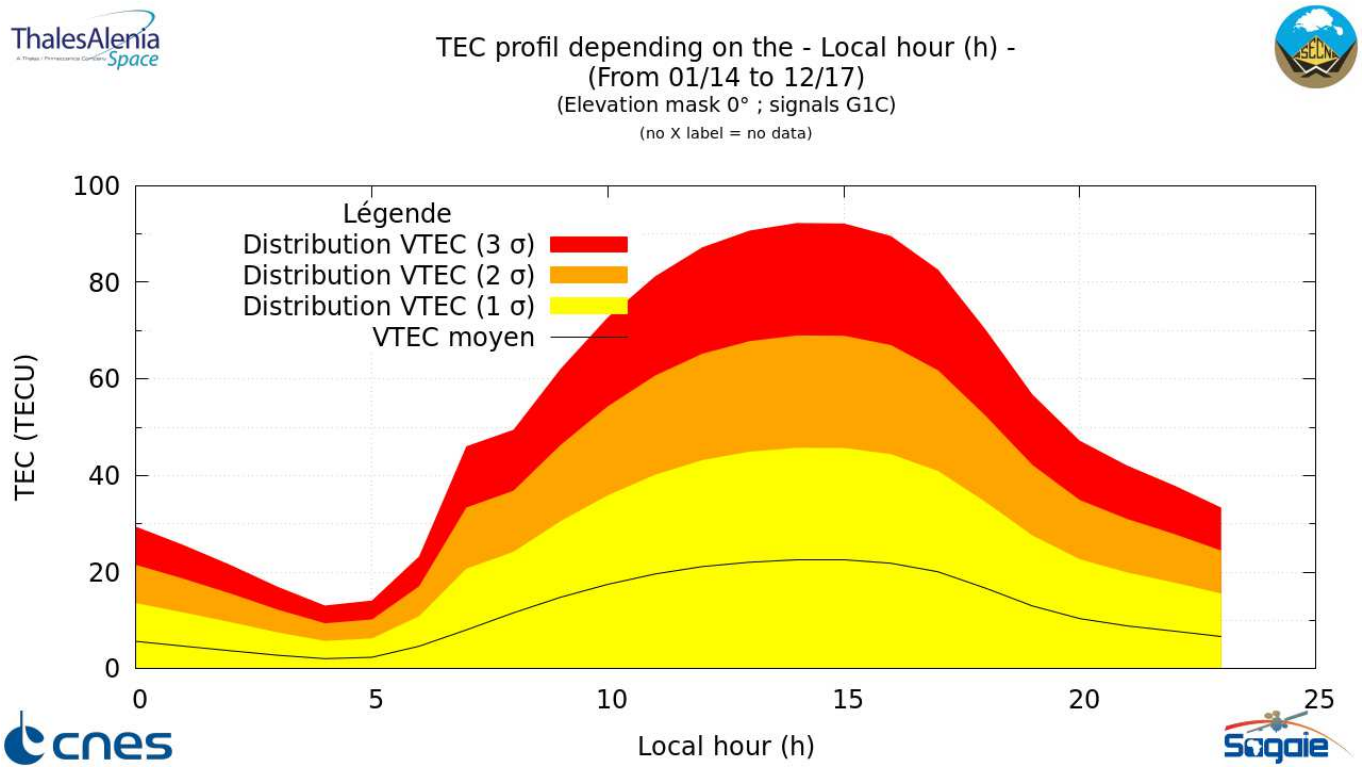

Figure 11: Hourly average TEC value from 2014 and 2017. Black line is $\|\boldsymbol{TEC}\|$, yellow array is $\|\boldsymbol{TEC}\| + \boldsymbol{\sigma}$, orange array is $\|\boldsymbol{TEC}\| + \boldsymbol{2\sigma}$ and red array is $\|\boldsymbol{TEC}\| + \boldsymbol{3\sigma}$.

In conclusion the TEC daily variation follows the solar zenith angle and temperature evolutions. A growth in TEC is observed between 6h LT and 15h LT, which corresponds to the maximum of solar flux received. Then between 15h LT and 6h LT, we observe a rapid decay of the TEC amplitude as the Sun sets and the night falls.

SHORT TERM FLUCTUATIONS

Short term variations study is important to characterize the limits in variation expected for the equatorial ionosphere. First, we present a study of Equatorial Plasma Bubbles, then the calculation of TEC gradients and finally we provide an estimation for the Along Arc TEC Rate (AATR).

Equatorial Plasma Bubbles Study & TEC Gradient Study

SBAS offers to provide an ionospheric correction based on a derived Grid Ionospheric Vertical Error (GIVE) calculation on Ionospheric Grid Point (IGC). Standard GPS ionospheric correction is derived from the Klobuchard model [13], which is a very simple model to approach ionosphere physical properties. Thales Alenia Space offers to reconstruct the local ionosphere using a TRIN (Triangular Interpolation) model, which is described in [14]. In order to provide good accuracy of the ionosphere TEC value locally around a grid point, a study of the TEC gradient variability is presented here, using all stations available during the period of time.

Temporal Variation

In this section, we present the temporal evolution of TEC above the sub-Saharan area, as it's a good estimation of how fast the ionosphere can evolve during a given amount of time. To ensure that a SBAS system is achievable there, slow variation of TEC should be expected. At least, temporal variation of TEC should be kept between the extrema values that can be simulated by the ionospheric model, in order to ensure a good correlation between the GIVE provided to a user and what is really observed.

To compute temporal TEC evolution, we have used the same idea developed in [15]. It aims to look at the difference of TEC measurement between the same LoS, measured at two different times but close. Consider a LoS i between a station and a satellite, at a time t and $t + dt$ then:

$$\nabla TEC_i = \frac{TEC_i(t + \delta t) - TEC_i(t)}{\delta t}$$

For our study, δt is set to 60 seconds. TEC time derivative distribution is presented in **Figure 12**. Values seem to follow an inverse law, as there is much more very small values of TEC gradients than high values, and the transition between the two is sharp. Mean temporal TEC gradient is about 0.003 TECU/s, 1 TECU is 16 cm of error in the f_1 pseudorange estimation. Meaning 0.003 TECU leads to a 0.048 cm error, which is well below the limits. We must also say that the ionospheric module is refreshed every 15 minutes which might lead to an error of estimated TEC of : $0.003 * (15 * 60) = 2.7$ TECU which is 43.2 cm of error on the f_1 pseudorange estimation.

Therefore, the equatorial ionosphere is showing rather slow variation in time, but the overall amplitude of these variations might be sufficient to rethink the refresh time for the GIVE estimation. A refresh time of 5 minutes would help minimizing the error.

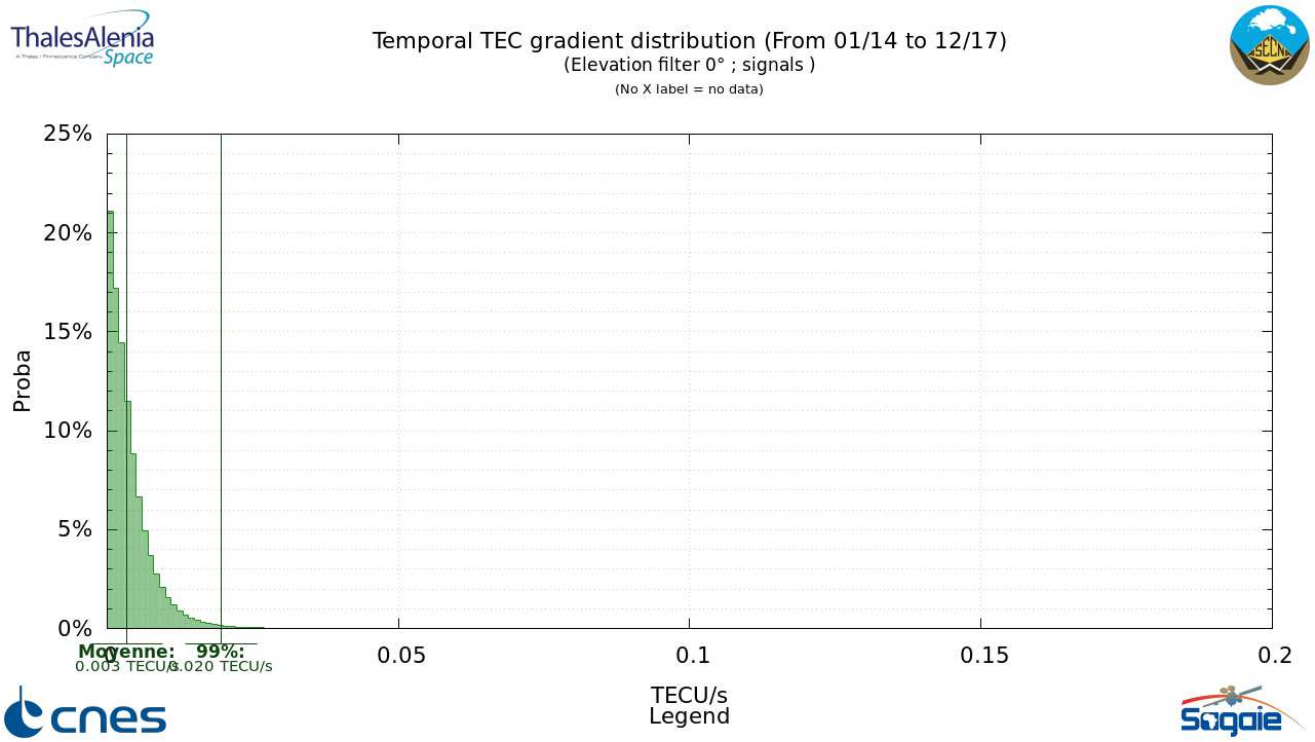

Figure 12: Temporal TEC distribution on sub-Saharan area, from 01/01/2014 to 31/12/17. TEC gradient are shown at the bottom, on the left side the probability to obtain a certain TEC gradient. Mean and 99% value are also shown.

Spatial Variation

In a second time, we have studied the evolution of spatial gradients. This one is very important because it will constrain the ionospheric model used for the interpolation problem. In the equatorial ionosphere, we can expect a slow varying ionosphere due to night and day variation but also a rapid one due to the presence of equatorial plasma bubbles. The latest one will cause the evening ionosphere to be unstable with altitude, as Rayleigh-Taylor instabilities might be present, generating plasma bubbles of enhanced (or depleted) electron density.

To measure the spatial TEC gradients, we have used two different methods, explained in the following. The first method consists in looking at one specific Spatial Variation of Ionosphere Delay (SVID) with two different stations, very close to each other. By doing so, the SVID is monitored at a given time t with two Ionospheric Pierce Points (IPP) and therefore two TEC measurements. The spatial TEC gradient can be calculated as followed:

$$\nabla TEC_{AB} = \frac{TEC_B(t) - TEC_A(t)}{\delta x}$$

Where A and B refers to two close stations, t is the time and δx is the baseline distance corresponding to the distance between the two stations. A scheme of this method is presented in **Figure *13***. But unfortunately, for our area of interest, all stations are in average 100 km away from each other, while this method works well for close stations (few meters away). We have therefore used the option 2 displayed in **Figure *14***.

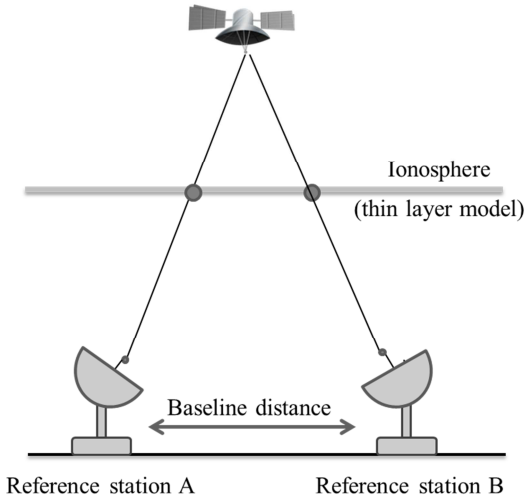

Figure 13: Spatial TEC gradient calculation using two stations close to each other

This is very similar to the method used for the temporal TEC gradient measurement. We focus on one SVID monitored by a station. The same line of sight is followed during a long time. The spatial TEC gradient is calculated as:

$$\nabla TEC = \frac{TEC(t + \delta t) - TEC(t)}{d}$$

Where t is the time, δt a given amount of time, here we take 300s and d is the distance between the two IPPs.

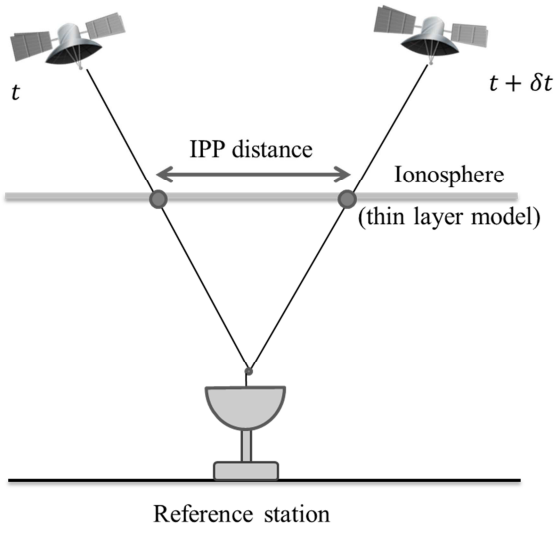

Figure 14: Spatial TEC measurement using long exposure time.

Spatial TEC gradients distribution is shown in **Figure *15***. Mean value of spatial TEC gradients is about 0.011 TECU/km. It means an error in TEC estimation of 0.011 TECU for two IPPs 1 km away from each other, which is a 0.176 cm error on the pseudo range estimation, still below the limits. But if we considered two IPPs 100 km away from each other, the error rises to a 17.6 cm error. To cover this variability, proper interpolation techniques for the GIVE estimation must be used and a wider stations network can be constructed. More ground stations will allow a better coverage of the spatial variations. As spatial variations are an issue for equatorial ionosphere, it is widely advised.

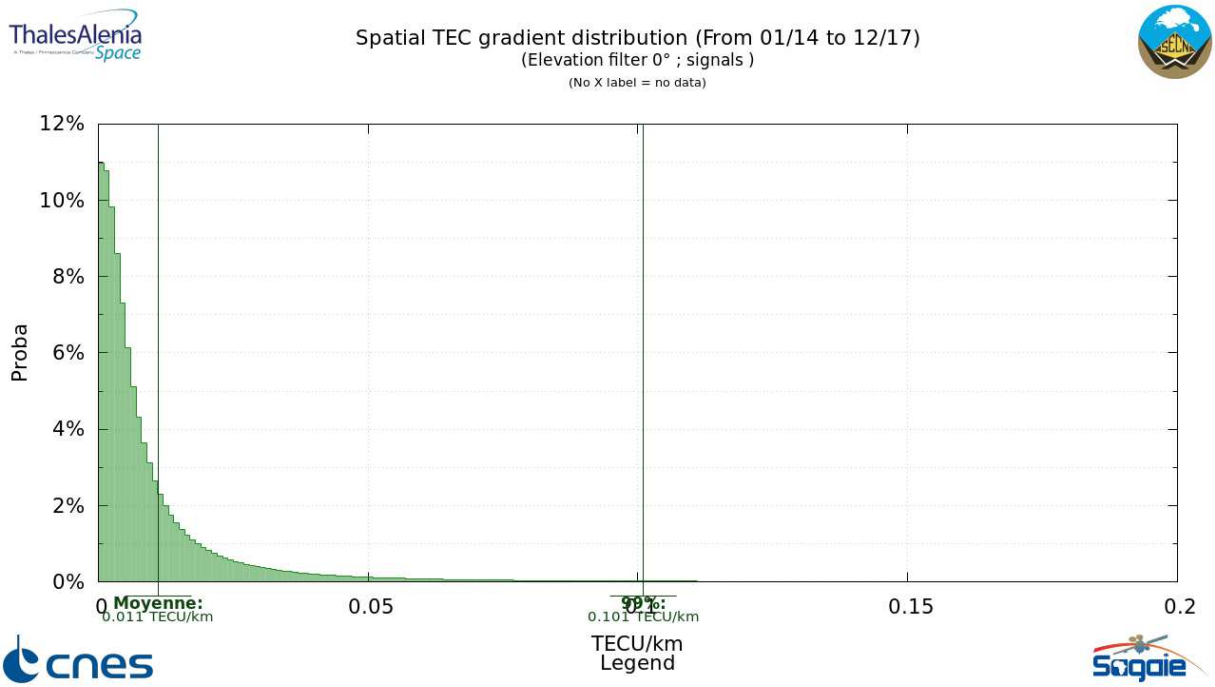

Figure 15: Spatial TEC gradients distribution on sub-Saharan area, from 01/01/2014 to 31/12/17. TEC gradient is shown at the bottom, on the left side the probability to obtain a certain TEC gradient. Mean and 99% value are also shown.

Along Arc TEC Rate Study

In this part, we study the Along Arc TEC Rate, which represents the TEC variations monitored by a LoS during time. The AATR estimation method is presented in the Method section. We present in **Figure *16***, the results of the AATR probability distribution on the sub-Saharan area from 2014 to 2017. The AATR probability distribution seems to follow an inverse law. The mean AATR value for this time interval is 3.80mm/s and the value equal to 99% of the distribution is 25.58mm/s. These values seem to follow ESA recommendations for AATR calculated on the equatorial region.

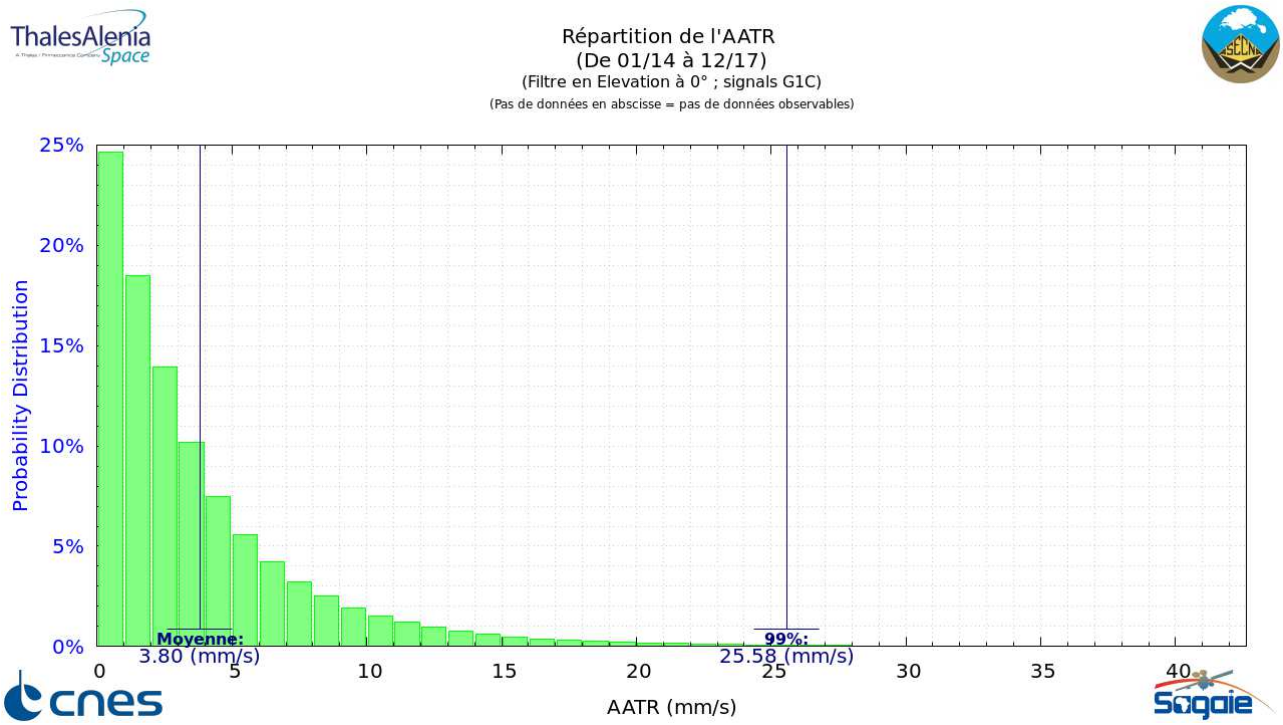

Figure 16: AATR profile on sub-Saharan area. AATR has been calculated for each line-of-sight monitored from 2014 to 2017 on the SAGAIE network. Mean value and 99% value are displayed on the graph.

The Root Mean Square (RMS) value of AATR has also been calculated for the same time interval. The AATR RMS value over one hour probability distribution is shown in **Figure *17***. The AATR RMS distribution seems to follow an inverse law with a mean value of 4.94mm/s. Previous study shows higher probability of very little AATR values, while using the RMS method, these values seems to have been filtered. The mean value is also higher which is in agreement with the equatorial ionosphere values given by ESA.

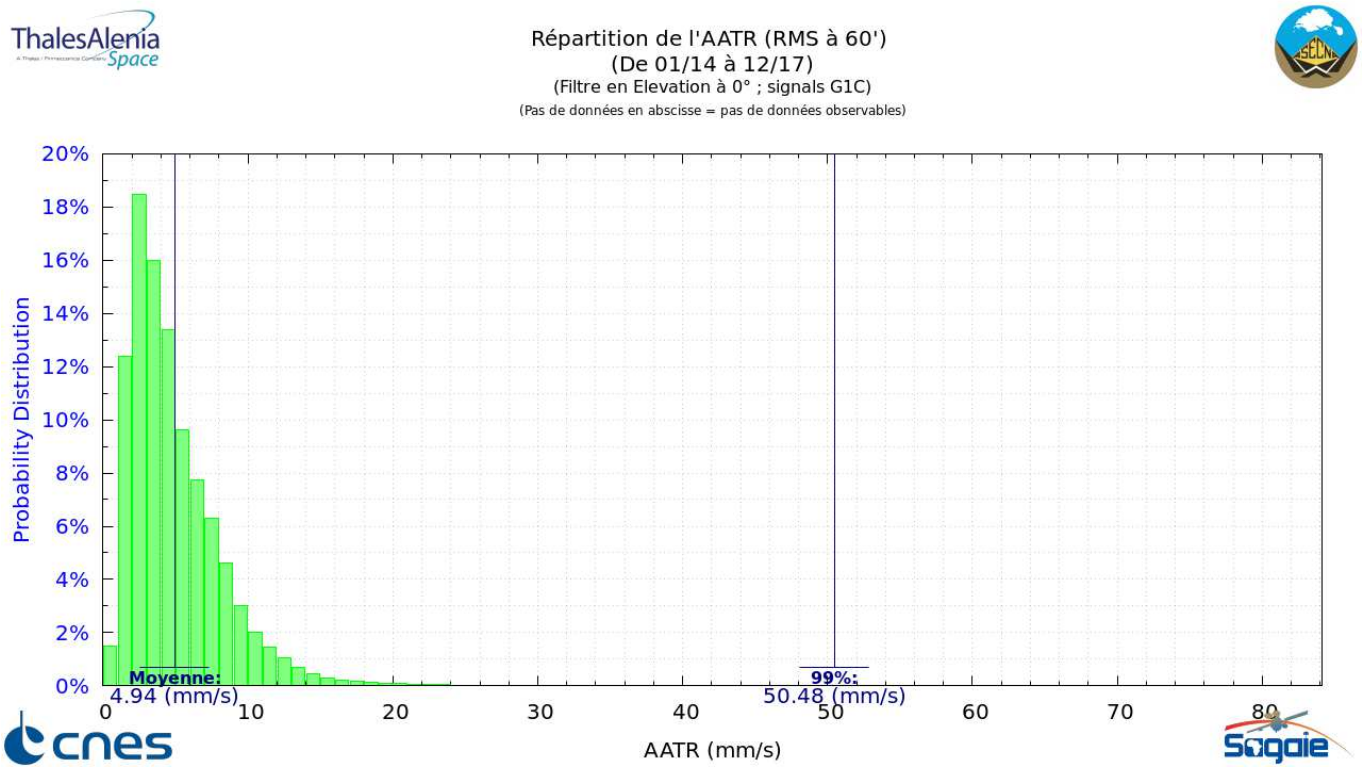

Figure 17: AATR RMS at one hour. AATR RMS has been calculated for each line-of-sight monitored from 2014 to 2017 on the SAGAIE network. Mean value and 99% value are displayed on the graph.

CONCLUSION

In order to characterize the equatorial ionosphere, a bibliographical work has been done to identify the main physical processes that take place at the equator. Knowing their main features in the ionosphere, it has been easier to understand the data monitored by the SAGAIE ground based network located on sub-Saharan area. From 2014 to 2017, the ground stations have monitored every raw measurement from the observable positioning satellites. With these data, we have been able to study the time and space variations of the ionosphere profiles. Higher TEC and scintillation amplitude have been found as expected for an equatorial ionosphere. Spatial and time TEC gradients seem to take reasonable values, given the geographical and physical processes at stake. This means that they can be well simulated by the Thales Alenia Space ionosphere module.

In conclusion, equatorial ionosphere shows much higher profile amplitude compared to mid latitude ionosphere, but it seems to stay in a reasonable range. Ionosphere model developed by Thales is able to well reproduce the main quantities profiles, and with the development of the SAGAIE network in the future, multiple data measurements will be added, in order to constrain even better these models.

ACKNOWLEDGMENTS

Authors would greatly like to thank CNES, owner of the SAGAIE network, for authorizing the use of SAGAIE data for this article. Thales Alenia Space would like to thank ASECNA's teams for their support in operating the SAGAIE network.

BIBLIOGRAPHY

[1] SAGAIE A GNSS Network for Investigating Ionospheric Behavior in Sub-Saharan Regions, Inside GNSS, september/october 2014, http://insidegnss.com/wp-content/uploads/2018/01/sepoct14-Monnerat.pdf.

[2] P. L. Blelly and D. Alcaydé, "Ionosphere," in *Handbook of the Solar-Terrestrial Environment*, Berlin, Springer, 2007, p. 190.

[3] P. Chamberlin, T. Woods and F. Eparvier, "Fare Irradiance Spectral Model (FISM): Daily component algorithms and results," *Space Weather*, no. 5, 2007.

[4] H. Lühr, S. Maus and M. Rother, "Nonn-time equatorial electrojet: its spatial features as determined by the CHAMP satellite," *JGR*, 2004.

[5] M. C. Kelley, The Earth's Ionosphere, San Diego, California: Academic Press, inc., 1989.

[6] L. F. Rezende, E. de Paula, I. Batista, I. Jelinek Kantor and M. Muella, "Study of ionospheric irregularities during intense magnetic storms," *Revista Brasileira de Geofísica*, pp. 151-158, 2007.

[7] H. Aveiro, D. L. Hysell, R. G. Caton, K. M. Groves, J. Klenzing, R. S. R. Pfaff and R. A. Heelis, "Three-dimensional numerical simulations of equatorial spread F: Results and observations in the pacific sector," *JGR*, 2012.

[8] V. Chauhan, O. Singh and B. Singh, "Diurnal and seasonal variation of GPS-TEC during a low solar activity period as observed at a low latitude station Agra," *Indian Journal of Radio and Space Physics*, pp. 26-36, 2011.

[9] J. Picone, A. Hedin, D. Drob and A. Aikin, "NRLMSISE-00 empirical model of the atmosphere: Statistical comparisons and sientific issues," *J. Geophys. Res.*, no. 107, p. 1468, 2002.

[10] M. R. Torr and D. Torr, "The seasonal behaviour of the F2-layer of the ionosphere," *Journal of Atmospheric and Terrestrial Physics*, pp. 2237 - 2251, 1973.

[11] B. Oryema, E. Jurua, F. D'ujanga and N. Ssebiyonga, "Investigation of TEC variations over the magnetic equatorial and equatorial anomaly regions of the African sector," *Advances in Space Research*, pp. 1939 - 1950, 2015.

[12] M. Aggarwal, "TEC variability near northern EIA crest and comparison with IRI model," *Advances in Space Research*, pp. 1221-1231, 2011.

[13] J. Klobuchard, "Ionospheric Time-Delay Algorithms for Single-Frequency GPS Users," *IEEE Transactions on Aerospace and Electronic Systems*, no. 3, pp. 325-331, 1987.

[14] P. Alleau, G. Buscarlet, S. Trilles, M. Van Den Bossche and B. J., "Comparative ionosphere Electron Content Estimation Method in SBAS Performances," Toulouse, 2011.

[15] A. J. Manucci, B. D. Wilson, Y. D. N., C. H. Ho, U. J. Lindqwister and T. Runge, "A global mapping technique for GPS-derived ionospheric total electron content meaurements," *Radio Science*, pp. 565-582, 1998.

[16] F. Gao, T. He, J. Masek, Y. Shuai, C. Schaaf and Z. Wang, "Angular Effects and Correction for Medium Resolution Sensors to Support Crop Monitoring," *IEEE Journal of Selected Topics in Applied Earth Observations and Remote Sensing*, pp. 4480-4489, 2014.